OPEN ACCESS

University of BRISTOL

Koyama, D., & Orr-Ewing, A. (2016). Triplet State Formation and Quenching Dynamics of 2-Mercaptobenzothiazole in Solution. *Physical Chemistry Chemical Physics*, *18*(37), 26224-26235. https://doi.org/10.1039/C6CP05110C

Peer reviewed version

Link to published version (if available):
10.1039/C6CP05110C

Link to publication record in Explore Bristol Research
PDF-document

This is the author accepted manuscript (AAM). The final published version (version of record) is available online via RCS at http://pubs.rsc.org/en/Content/ArticleLanding/2016/CP/C6CP05110C#!divAbstract. Please refer to any applicable terms of use of the publisher.

University of Bristol - Explore Bristol Research
General rights

This document is made available in accordance with publisher policies. Please cite only the published version using the reference above. Full terms of use are available:
http://www.bristol.ac.uk/red/research-policy/pure/user-guides/ebr-terms/

Please do not adjust margins

Journal Name

ARTICLE

Triplet State Formation and Quenching Dynamics of 2-Mercaptobenzothiazole in Solution

Daisuke Koyama and Andrew J. Orr-Ewing*

Received 00th January 20xx,
Accepted 00th January 20xx

DOI: 10.1039/x0xx00000x

www.rsc.org/

The photochemical dynamics of the thione 2-mercaptobenzothiazole (MBT) initiated by absorption of 330-nm ultraviolet light are investigated by ultrafast transient absorption spectroscopy. The lowest energy triplet state (T_1) has mixed $^3\pi\pi^*$ / $^3n\pi^*$ character and is populated with a quantum yield of 0.58 ± 0.01 from the photo-excited $^1\pi\pi^*$ S_2 state in methanol solution via rapid internal conversion to the $^1n\pi^*$ S_1 state (with time constant $\tau_1 < 150$ fs). The spectroscopic evidence points to a mechanism involving intersystem crossing from S_1 to the $^3n\pi^*$ / $^3\pi\pi^*$ T_2 state ($\tau_2 = 400 \pm 100$ fs) and internal conversion to T_1 (with time constant for growth $\tau_3 = 6.1 \pm 0.4$ ps). The remainder of the photoexcited molecules return to the ground state by $S_1 \rightarrow S_0$ internal conversion. In methanol solution, the T_1 state is long-lived but when the solvent is changed to styrene, triplet quenching is observed with a time constant of 107 ± 8 ps and assigned to the adduct-mediated energy transfer process MBT (T_1) + Styrene (S_0) → ^{3}[MBT-Styrene] → MBT (S_0) + Styrene (T_1). Transient vibrational absorption spectroscopy observes the ^{3}[MBT-Styrene] biradical intermediate and determines its lifetime to be 700 ± 80 ps. Computational studies identify the mechanistic pathway for triplet quenching, which involves a curve crossing between two triplet states of the MBT-Styrene adduct. The quenching process occurs with high efficiency, and no long-lived isomers of the initial adduct are observed.

1. Introduction

2-Mercaptobenzothiazole (MBT) and its derivatives such as the corresponding disulfide, 2,2'-dithiobis(benzothiazole) (BSSB) and sulfenamides are essential chemical compounds for the rubber industry as accelerators for vulcanization.[1] Recently, we reported observation of the photo-induced reactions following BSSB photodissociation in solutions containing an alkene:[2] a combination of ultrafast transient electronic absorption spectroscopy (TEAS) and transient vibrational absorption spectroscopy (TVAS) revealed a comprehensive picture for the initial steps of a thiol-ene reaction, a class of reactions finding use in "Click Chemistry".[3] Industry also uses MBT as a corrosion inhibitor for metals, in some cases under atmospheric conditions where MBT is degraded by exposure to sunlight.[4] The photodegradation of MBT has therefore been investigated previously using microsecond-timescale flash photolysis and mass spectrometry.[4, 5]

Here, we focus on the photochemical dynamics of MBT on the sub-picosecond to picosecond timescales and report detailed mechanisms for triplet state formation and quenching in an alkene solution. In contrast to simpler thiol compounds, the photochemical dynamics of MBT are significantly different from the disulfide, reflecting a contribution from the thione (thiocarbonyl) form. Two possible tautomeric forms for MBT derive from its N-atom containing structure, the thione and the thiol forms which are shown below. The thione form is strongly favoured in both the gas and liquid (water) phases at room temperature.[6-9]

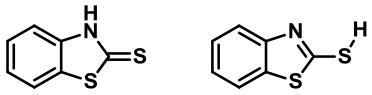

thione form thiol form

The photochemistry of thione compounds is well-studied, and it is widely accepted that the first triplet excited state (T_1) plays a major role in their photochemical reactions.[10, 11] The thione triplet excited state is thought to be efficiently formed though ultrafast intersystem crossing (ISC) from the first singlet excited state (S_1), in contrast to slower ISC in the corresponding oxygen-atom containing compounds, because of the larger spin-orbit coupling derived from the sulfur atom.[12, 13] The S_1 state has optically "dark" $n\pi^*$ character in the Franck–Condon region, but can be populated by internal conversion (IC) from the second excited singlet state (S_2) which is optically bright and has $^1\pi\pi^*$ character.[14, 15] Ultrafast thione T_1 state formation dynamics have been investigated by TEAS, as well as by *ab initio* electronic structure calculations and surface hopping simulations that include spin-orbit coupling.[16-27] The emerging

School of Chemistry, University of Bristol, Cantock's Close, Bristol BS8 1TS, UK
E-mail: A.Orr-Ewing@bristol.ac.uk; Tel: +44 (0)117 9287672

† Electronic Supplementary Information (ESI) available: All experimental data are archived in the University of Bristol's Research Data Storage Facility (DOI 10.5523/bris.1thhavttjbiuh1prrexbyu1d7w). The Supplementary Information contains plots of molecular orbitals of MBT thione and thiol forms; computed vertical excitation energies and transition dipole moments for the MBT thiol form; steady state UV/vis spectra of MBT in styrene solution and pure styrene; TEA spectra of MBT in toluene solution; an example of spectral decomposition of TEA spectra in methanol solution; computed PECs for MBT; steady state FT-IR spectra of MBT in styrene and of pure styrene; an example of spectral decomposition of TVA spectra in toluene solution; computed fundamental infrared transition frequencies for MBT excited states; simulated UV/vis spectra for triplet styrene and ^{3}[MBT-St]; computed infrared frequencies and energy diagrams for the addition products; TEA and TVA spectra of thioxanthone in methanol and styrene solutions; and calculated fundamental infrared band positions for triplet styrene. See DOI: 10.1039/x0xx00000x

This journal is © The Royal Society of Chemistry 20xx

Please do not adjust margins

Please do not adjust margins

picture is of a complicated competition between IC and efficient ISC.

Triplet state thione compounds take part in various types of intermolecular interactions, such as energy transfer, addition to alkenes, electron transfer, and hydrogen atom abstraction.[10, 28, 29 30, 31] The current study combines TVAS and TEAS measurements to map out the pathways for population of the MBT T_1 state and its quenching by styrene. We identify spectroscopic signatures of excited electronic states and reaction intermediates, from which we determine that the triplet state of MBT is quenched through a short-lived adduct with an alkene molecule, ^{3}[MBT-styrene].

2. Experimental Details

2.1. Transient Absorption Spectroscopy

The ultrafast laser system used for transient absorption spectroscopy experiments, and the procedures for accumulating TEAS and TVAS measurements have been described previously.[32] We therefore concentrate here on details specific to the current study.

Photochemistry of MBT was studied in solutions of methanol, toluene (both Analytical Grade, Sigma Aldrich) and styrene (≥ 99%, Sigma Aldrich). 2-Mercaptobenzothiazole (97%, Sigma Aldrich) was recrystallized from methanol/chloroform (Analytical Grade, Sigma Aldrich) solution prior to use. Methanol and toluene were used as received, but the styrene was passed through a basic aluminium oxide column before use to remove the inhibitor, 4-*tert*-butylcatechol.

Transient absorption measurements used a Harrick cell with CaF_2 windows separated by a PTFE spacer (380-μm thickness for TEAS and 100-μm thickness for TVAS experiments) through which sample solutions were circulated by a peristaltic pump. The UV excitation wavelength was 330 nm for both TEAS and TVAS experiments. Concentrations of the MBT solutions were adjusted to give an optical density (OD) of ~0.5 at 330 nm at the given spacer thickness (0.56 mM for TEAS and 2.1 mM for TVAS measurements). The UV excitation wavelength was chosen to avoid strong absorption by styrene and to populate the second excited state ($\pi^* \leftarrow \pi$ transition) of MBT. The absorption ratio at 330 nm for styrene / MBT is less than ~0.01 under our experimental conditions. The pump laser energy was adjusted to 800 nJ / pulse to suppress multiphoton absorption processes. All experiments were carried out with an air head-space in the sample reservoir, and without purging O_2 from the sample solutions, because preliminary tests under an inert atmosphere showed no influence from molecular oxygen on the TEAS spectral band shapes or reaction kinetics on picosecond timescales. For TEAS experiments, the pure solvents (methanol, toluene and styrene) showed transient response signals which contributed background signals to the recorded spectra.[2] Hence, the solvent-only TEA spectrum at each time delay was subtracted from the corresponding MBT-solution spectrum to eliminate contributions from the solvent.[2] The instrument response function (IRF) for TEAS experiments was 150 fs,[2] and a 300-fs IRF for TVAS experiments was limited by thermal lensing effects.

2.2. Computational Methods

Calculations of infrared frequencies and thermodynamic parameters for all species of interest were performed using the Gaussian 09 package.[33] The B3LYP density functional,[34, 35] with the 6-311++G(3df,3pd) basis set was chosen. Computed infrared band positions were corrected using a linear function obtained by comparing experimental and calculated frequencies for 2,2'-dithiobis(benzothiazole).[2] This procedure gives good agreement (see below) between experimental TVAS and computed frequencies for the compounds and intermediates of interest here, across our mid-IR probe region.

Separation-dependent potential energy curves (PECs) for MBT (T_1) + Styrene (S_0), MBT (S_0) + Styrene (T_1), and a MBT (S_0) + Styrene (T_1) complex were obtained using the CAM-B3LYP density functional with D3 dispersion correction (CAM-B3LYP-D3),[36, 37] with the 6-311+G(d,p) basis set. The first two PECs were obtained by locating transition state geometries and then scanning the C-S bond distance with contact angles frozen at the transition state geometries. Fully relaxed PEC scans were used in the calculations of the MBT (S_0) + Styrene (T_1) complex pathway.

Vertical excitation energies and transition dipole moments of the thione form of MBT were calculated using the Molpro package.[38] The calculation used the state averaged complete active space self-consistent field (SA-CASSCF) method with the aug-cc-pVTZ basis set. The geometry was optimized with the Gaussian 09 package using Møller-Plesset second-order perturbation theory (MP2) and the aug-cc-pVTZ level of theory.[39, 40] Complete active space with second-order perturbation theory (CASPT2) energies were calculated using the SA-CASSCF result as a reference wavefunction. An imaginary level shift of 0.4 a.u. was used for all of the CASPT2 calculations to avoid intruder state problems. These calculations included eight electrons in seven active orbitals (8/7) comprising the non-bonding thione S orbital, three π and the three corresponding π* orbitals. These orbitals are illustrated in Figure S1 of Supplementary Information (SI) as numbers 40 - 46. The choice of active space was tested and validated against calculations which used a larger 12/10 active space including π and π* MOs localized on the benzene ring and delocalized across the two rings.

3. Results and discussion

We begin with a brief interpretation of steady state UV/vis spectra of the MBT solutions followed by the results of TEAS and TVAS experiments. TEAS measurements reveal the population and decay of the MBT S_1 and T_1 states, whereas TVAS measurements, combined with electronic structure calculations of vibrational band frequencies, unravel the chemical identities of intermediates and photo-products.

Figure 1 shows a steady state UV-vis spectrum of 0.56 mM MBT in methanol. The strongest absorption band peaks at 325 nm, and the molar extinction coefficient at our 330-nm pump laser wavelength is $\varepsilon_{330nm} = 23300 \pm 200\ M^{-1}\,cm^{-1}$. This value is comparable to the maximum extinction coefficient at 315 nm in aqueous solution.[5] Computed vertical excitation wavelengths (which are not corrected for solvent effects) and transition dipole moments (TDMs) provided in Table 1 indicate that the lowest singlet excited state S_1 has nπ* character, but is an optically "dark" state, as is typical for thione (or ketone) compounds. The lowest singlet optically "bright" excited state is the S_2 state, for which the computed vertical excitation wavelength from the S_0 state is 336 nm, a value in reasonable agreement with the experimental peak absorption. The

 This journal is © The Royal Society of Chemistry 20xx

Please do not adjust margins

Please do not adjust margins

calculated vertical excitation energies suggest that the $S_3 \leftarrow S_0$ transition will appear at 322 nm, with a TDM similar to that for the $S_2 \leftarrow S_0$ excitation. Hence, the asymmetric shape of the band in the UV/vis spectrum centred at 325 nm can be understood to result from overlap of these two absorption features. Nevertheless, the chosen 330-nm UV excitation wavelength for our experiments favours initial population of the S_2 state.

As was mentioned earlier, MBT has two possible tautomeric forms, with the thione form reported to be dominant.[6-9] Vertical excitation energies and transition dipole moments for the thiol form of MBT were therefore also calculated (see Table S1 of SI), and indicate that the thiol form does not absorb at wavelengths around 330 nm. Although the precise thione : thiol tautomer ratio in methanol is uncertain, the 330-nm UV light predominantly excites the thione form and we concentrate on the photochemistry of this tautomer. Comparison of the UV/visible spectrum of MBT in styrene and methanol solutions shows that the thione tautomer is also responsible for 330-nm light absorption in measurements conducted in styrene (Figure S2 of SI).

3.1. Triplet State Production Dynamics of MBT following 330-nm UV excitation

The mechanism for population of the MBT lowest triplet state is unravelled by a combination of TEAS and TVAS, supported by electronic structure calculations. TEA spectra of MBT in methanol and toluene showed similar band features and kinetics, but we focus on the measurements in methanol solution for which the short-time dynamics are most clearly resolved. An interfering transient signal from pure methanol was only seen while the pump and probe pulses overlapped in time, in contrast to the other pure solvents in which transient signals lasted for longer than 1.3 ns in toluene and ~24 ps in styrene.[2] TEA spectra in toluene are reported in Figure S3 of the Supplementary Information, and the measurements in styrene are discussed in Section 3.2.1. Transient absorption signals extended to wavelengths as long as 625 nm, but features located at wavelengths shorter than ~350 nm were masked by the UV-pump laser light.

TVAS experiments were performed for MBT over the probe wavenumber range 1240 - 1450 cm^{-1} in both toluene and styrene solutions (Section 3.2.2) following 330-nm UV excitation. The TVAS measurements for MBT in toluene identify a pathway for the MBT T_1 production. No transient absorption from pure toluene is observed in this IR spectral region when subjected to the 330-nm pump light.[2]

3.1.1. TEAS of MBT in methanol solution. Figure 2 shows TEA spectra of MBT in methanol. A prominent band centred at 557 nm is evident in Figure 2(a), and has a constant integrated band intensity after ~20 ps. This spectral feature is different from that reported for the benzothiazole-2-thiyl radical,[2] and we assign it to absorption from the T_1 state of MBT. This assignment is guided by the resemblance of the spectral band shape to the reported spectrum for the T_1 state of MBT in water, obtained by microsecond flash photolysis and confirmed by molecular oxygen and methyl acrylate quenching experiments.[5] Further analysis of the spectra, and decomposition into contributions from different electronic bands, used the KOALA program.[41] Figure 2(b) illustrates the early time features, and the time dependences of the observed bands are shown in 2(c). The T_1 band centred at 557 nm grows with time constants of τ_1 = 0.4 ± 0.1 ps and τ_2 = 6.3 ± 0.4 ps deduced by exponential fits to time-dependent band intensities combined with Gaussian convolution to account for the IRF of 150 fs.[2] This kinetic behavior either suggests that there are two pathways for the population of the T_1 state, or that there is a spectrally overlapped intermediate electronic state absorption which grows with time constant of 0.4 ps and decays with time constant of 6.3 ps, yielding the T_1 state. TVAS experiments discussed in Section 3.1.2 indicate that the T_1 population grows on a time scale of 5 ps. Therefore, we conclude that the second interpretation of the growth of the 557-nm band is plausible and propose that the faster time constant corresponds to ISC from the S_1 state to the T_2 state, whereas the slower rise represents IC from the T_2 to the T_1 state. Evidence in support of this proposed mechanism is presented below.

The kinetic behavior in the spectral region around 370 nm clearly differs from that for the band at 557 nm. In particular, the band intensity at 370 nm reaches its maximum during the instrument response time and then decays. The 330-nm pump wavelength excites the S_2 state, and theoretical simulations using surface-hopping methods for other thione compounds (*e.g.*, 6-thioguanine and 2-thiouracil) suggest that internal conversion from the thione S_2 to S_1 state is almost barrierless and ultrafast (< 100 fs).[17, 21] Hence, it is likely that S_1 excited-state absorptions contribute to the TEA spectra at our earliest measurement times. The 370-nm band decays with time constants of τ_1 = 0.4 ± 0.1 ps and τ_2 = 5.9 ± 0.3 ps (Figure 2(c)), and thereafter shows a constant absorbance until the limit of our experimental time delay. The two time constants for the decay are consistent with the rise of the band intensity at 557 nm, within the 2 SD fit uncertainties. Furthermore, the long lived component of the absorption around 370 nm suggests a contribution from an overlapping triplet state absorption band.

The TEA spectra can be decomposed into three contributing components well-represented by our observed bands at time delays of 200 fs (assigned to the S_1 absorption), 2.0 ps (assigned to T_2 absorption, on the basis of evidence from TVAS data presented later), and 100 ps (when the T_1 absorption is the sole contributor). Using these basis spectra as fitting functions, we performed a spectral decomposition within the KOALA program[41] (exemplified in Figure S4 of the Supplementary Information) and the outcomes (without normalization) are shown in Figure 2(d). The solid lines in the figure are obtained by a global fitting of the three sets of integrated band intensities to an integrated rate expression appropriate for the scheme in Equation (1), in which the absorption and $S_2 \rightarrow S_1$ IC steps are too fast to resolve, giving $\tau_1 = 1/k_1 = 0.5 \pm 0.1$ ps and $\tau_2 = 1/k_2 = 7.2 \pm 0.4$ ps.

$$\mathrm{MBT\ S_0} \xrightarrow{h\nu} \mathrm{S_2} \xrightarrow{\mathrm{IC}} \mathrm{S_1} \xrightarrow{k_1} \mathrm{T_2} \xrightarrow{k_2} \mathrm{T_1} \qquad (1)$$

The assignment of the τ_1 and τ_2 values is uniquely determined because the decay of the S_1 state absorption and the rise of the T_1 state absorption are both observed. The fitting result matches the extracted band intensities satisfactorily, and the two time constants are in reasonable agreement with the observed time constants obtained by biexponential fitting.

Please do not adjust margins

Please do not adjust margins

To explore further the pathway for population of the T_1 state, MBT potential energy curves were calculated. The outcomes of these calculations are summarized in the Supplementary Information and shown in Figure S5. The S_1 and T_2 states are close to degenerate over most of the explored configuration space, supporting the above kinetic model which includes fast ISC from the S_1 to the T_2 state. The same route has been suggested as the main pathway for T_1 formation in other thione compounds on the basis of *ab initio* simulations.[17, 21] The transition from the S_1 state to the T_2 state of MBT, both of which have nπ* character in the Franck–Condon region, is nominally forbidden by the El Sayed rules.[42] However, the CASSCF calculations predict that at their equilibrium geometries, the T_1 state has mixed nπ* and ππ* character, whereas the T_2 state is mostly ππ* in character. Non-adiabatic transitions may occur from the vicinity of the minimum in the S_1 state, where both T_1 and T_2 states have mixed nπ* and ππ* character: the CASSCF calculations indicate that at the S_1 minimum geometry, the T_1 state is comprised of 34% nπ* and 54% ππ* character, whereas the T_2 state is 58% nπ* and 31% ππ* in character. In both cases, the remaining percentage is of other orbital character. The associated molecular orbitals are shown in Figure S1 of Supplementary Information. ISC from the S_1 state to the T_2 state therefore does not contravene the El-Sayed selection rules in the vicinity of the S_1 minimum.

The 6-ps time constant for $T_2 \rightarrow T_1$ IC appears, at first sight, to be slow for a spin-allowed transfer of population between two electronically excited states. We therefore also considered two other candidates for the slower time constant. These alternatives are solvation by methanol molecules or relaxation of vibrationally hot T_1 molecules produced either by direct $S_1 \rightarrow T_1$ intersystem crossing, or via the T_2 state with fast (< 6 ps) $T_2 \rightarrow T_1$ internal conversion. Either of these processes could account for the observed shift in the position of the band at 557 nm from higher to lower wavelength with a time constant of 6.6 ± 0.3 ps. However, our preferred assignment of the 6-ps time constant is to internal conversion from the T_2 to the T_1 state for three reasons. The first is the good agreement between the time constants for the growth of the T_1 state absorption and the slower component of the decay of the feature at 370 nm. The second reason is the isosbestic point observed at 600 nm in Fig. 2(a) and Fig. S4, which suggests evolution from one absorbing electronic state to another (e.g. $T_2 \rightarrow T_1$). The isosbestic point wavelength does not move with time, indicating two time-invariant spectral components. In contrast, solvent stabilization effects or vibrational cooling are expected to shift the whole band to shorter wavelength with increasing time delay. The third piece of evidence in support of our assignment derives from the TVAS measurements in toluene solution discussed in Section 3.1.2 which provide independent evidence for decay of a T_2-state band and growth of a T_1-state band on this ~6 ps time scale. If our assignment is correct, the rate of the $T_2 \rightarrow T_1$ IC appears to be limited by the accessibility of conical intersections between the two triplet states.

3.1.2. TVAS of MBT in toluene solution. Figure 3 shows TVA spectra of 2.1 mM MBT in toluene following 330-nm excitation, as well as integrated band intensities of features seen at 1318, 1364, 1370 and 1414 cm^{-1}. Two prominent negative bleach bands at 1414 cm^{-1} and 1318 cm^{-1}, and three relatively small bleach bands at 1268, 1283 and 1432 cm^{-1} are attributed to reduction in the ground-state MBT concentration induced by the pump light, and the assignments are confirmed by comparison with steady state FTIR spectra (Figure S6 of SI). The parent MBT bleach bands at 1318 and 1414 cm^{-1} recover with respective time constants of 11 ± 1 ps and 12 ± 1 ps, and thereafter (57 ± 1)% and (59 ± 1)% of the initial band depletions remain over our experimental time window. Assuming that internal conversion from the S_2 state to S_1 state is ultrafast and proceeds with a quantum yield of almost unity, as discussed earlier and suggested for other thione compounds,[17, 19] the decay with time constant of 11 - 12 ps can be ascribed to internal conversion from the S_1 state to the S_0 ground state through S_0 (v>0) levels, where v>0 represents excited vibrational states of the ground electronic state. The time constant is dominated by vibrational cooling because the S_1 state lifetime determined by TEAS is only 0.4 ps.

A quantum yield for the T_1 state of $\Phi(T_1) = 0.58 \pm 0.01$ is deduced by taking an average of the two values for persistence of the ground-state bleach. This analysis assumes that quantum yields for fluorescence from the short-lived S_2 and S_1 states are negligible, which is consistent with reports for other thione compounds.[12, 43] The observed time constant of 0.4 ps in TEAS experiments for loss of the S_1 state is therefore determined by both the $S_1 \rightarrow S_0$ (v>0) IC pathway and ISC to the triplet manifold in almost equal measure. Evidence presented below points to the T_2 state being a gateway to the T_1 state.

The $\Phi(T_1)$ value is lower than for other thione compounds, in which quantum yields for intersystem crossing are reported to be almost unity.[20, 43, 44] Variations in T_1 quantum yields reflect subtle differences in the ultrafast ISC versus IC dynamics, which were not directly probed in the prior studies using microsecond flash photolysis.

Careful inspection of the TVA spectra identifies a growing feature at 1370 cm^{-1} with an exponential time constant of 4.8 ± 0.8 ps (Figure 3(c)). The band shows a constant intensity after reaching its maximum (Figure 3(b)). We assign this band to the T_1 state of MBT on the basis of its time-dependence and wavenumber: the time-constant for growth of the band is consistent with TEAS measurements of the T_1 feature (Section 3.1.1), and computed infrared band positions for T_1 MBT reported in Table 2 predict a feature at 1372 cm^{-1}. The band at 1370 cm^{-1} is weak when compared to the depths of ground state bleach features (Figure 3), but its low intensity is compatible with a T_1 quantum yield of ~0.58 because the computed band intensity (Table 2) is much smaller than those for the S_0 bands.

We now focus on TVA spectra at earlier time delays highlighted in Figure 3(c). Two transient bands are seen at 1364 cm^{-1} and 1380 cm^{-1} at time delays of 0.4 - 2 ps. Spectral decomposition with the KOALA program,[41] examples of which are provided in Figure S7 of the SI, suggests that the band intensity at 1364 cm^{-1} reaches its maximum at a time delay of ~1 ps and decays completely within ~20 ps. Fitting of the integrated band intensity to the sequential kinetic model of eqn 1 gives $\tau_1 = 1/k_1 = 0.4 \pm 0.1$ ps for the growth of the band and τ_2

This journal is © The Royal Society of Chemistry 20xx

Please do not adjust margins

= $1/k_2$ = 6.1 ± 0.7 ps for the decay. These values agree with time constants deduced from TEAS experiments. We assign the band at 1364 cm^{-1} to MBT T_2 absorption on the basis of its separation from the T_1 band and comparison with computed infrared frequencies provided in Table S2 of the SI, as well as the observed time dependence. This assignment influences our interpretation of the early-time TEA spectra, as discussed in Section 3.1.1. The T_2 band is located to the lower frequency side of the T_1 band, and its decay timescale (~6 ps) is comparable to typical timescales for vibrational relaxation in solution.[2, 45] It could therefore be interpreted as deriving from vibrationally hot T_1 molecules produced by direct ISC from the S_1 state (with τ = 0.4 ps). However, the band position at 1364 cm^{-1} and its shape do not change for at least the first 2 ps, as is demonstrated in the inset to Figure 3(c). We therefore consider this alternative assignment of the band at 1364 cm^{-1} to vibrationally excited T_1 molecules to be less likely, because any hot band absorption should show a characteristic continuous shift to higher wavenumber as the vibrational excitation relaxes. The similarity in peak absorbances of the bands assigned to the T_2 and T_1 states, and their comparable computed band intensities (Table S2) support a mechanism in which the T_2 state is populated by ISC more rapidly than it decays to T_1 by IC.

The band at 1380 cm^{-1} reaches its maximum intensity within our experimental time resolution. It then decays on a timescale estimated to be ~2 ps, but spectral overlap with the T_1 band and an unresolved underlying T_2 feature prevented reliable spectral decomposition and more precise kinetic fitting. This band is tentatively assigned to the S_1 state on the basis of its kinetic behaviour and spectral location (see Table S2).

The kinetic trace for the T_1 band at 1370 cm^{-1} shown in Figure 3(b) and the spectral decomposition illustrated in Figure S7 of the SI indicate that the T_1 state is already weakly populated at the earliest time points in our measurements. A direct ISC pathway from either the S_2 or the S_1 state to the T_1 state is implied, but is judged to be a minor route to the MBT T_1 state on the basis of the time-dependent band intensities plotted in Figure 3(b). Figure 4 summarizes the main route to population of the MBT T_1 state, along with competing relaxation pathways following 330-nm excitation, as deduced from the TEAS measurements in methanol and TVAS in toluene.

3.2. Triplet State Quenching Dynamics of MBT in Styrene Solution following absorption of 330-nm UV light

The TEAS and TVAS data presented in section 3.1 establish the mechanism, timescales and quantum yield for production of T_1 state MBT after absorption of 330-nm light. The transient spectra were obtained in solvents that were non-quenching and unreactive towards the T_1 state on the $\leq$ 1.3 ns timescales of our measurements. We now examine the dynamics of quenching and reactive removal of the MBT T_1 state in styrene solution using the same spectroscopic methods. The TEAS study mainly reveals the decay dynamics of the T_1 state, whereas the TVAS measurement characterize intermediate species.

3.2.1. TEAS of MBT in styrene solution. TEA spectra of MBT in styrene are shown in Figure 5(a), and at early time delays resemble those observed for solutions of MBT in methanol and toluene, except for a slight red-shift of the band at 571 nm compared to the methanol solution. However, the observed kinetics at 571 nm and 370 nm are dramatically different from those seen in methanol and toluene, as Figure 5(b) illustrates. For example, the former band decays with a time constant of 105 ± 2 ps after reaching its maximum absorbance at ~15 ps, and completely disappears after ~400 ps. In contrast, the 370-nm band decays sufficiently slowly to last for longer than the limit of our experimental time delays. The slow-decay component is most evident as a band peaking near 370 nm and extending to 450 nm, but the later time-delay spectra suggest it may also contain a weak and broad absorption from 450 - 600 nm (see Figure 5(c) for a TEA spectrum at a time delay of 800 ps). Spectral decomposition with the KOALA program, an example of which is provided in Figure 5(c), demonstrates that the slow-decay component initially grows with time and reaches its maximum absorption intensity at ~200 ps. The band thereafter decays gradually, and approximately 25% of the maximum intensity remains after 1.3 ns. This kinetic behavior is indicative of formation of an intermediate species which relaxes to a stable product. The absence of this intermediate in the toluene or methanol solutions suggests either a reaction of the MBT T_1 state with styrene, or a solute - solvent energy transfer process specific to styrene solutions is taking place.

We propose that the growth of the band at 370 nm is a signature of the reaction of the MBT T_1 state with styrene (St), yielding a triplet state biradical addition product (denoted as ^{3}[MBT-St] and responsible for the 370-nm absorption), and the decay corresponds to dissociation of the ^{3}[MBT-St] to singlet MBT and triplet state St. This scheme is shown in Equation 2. Further evidence for these processes derives from analysis of TVAS measurements and is presented in Section 3.2.2.

$$^3\mathrm{MBT} + {}^1\mathrm{St} \xrightarrow{k_3} {}^3[\mathrm{MBT-St}] \xrightarrow{k_4} {}^1\mathrm{MBT} + {}^3\mathrm{St} \qquad (2)$$

A fit of the extracted kinetics at 370 nm to this model gives τ_4 = $1/k_4$ = 629 ± 41 ps by fixing τ_3 = $1/k_3$ = 105 ps obtained from the decay of the band at 571 nm.

The reaction scheme of eqn 2 suggests that an absorption from triplet styrene might contribute to the observed spectra at the later time delays. Prior reports of the absorption spectra of triplet styrene in cyclohexane, benzene and toluene show an absorption maximum at 320 nm, with a shoulder extending up to ~360 nm.[31, 46] A substantial shift to longer wavelength would be required in styrene solution to account for the weak features we see at wavelengths up to 450 nm and we therefore discount assignment of the observed later-time visible bands to triplet styrene. Instead, we prefer the proposed assignment to the adduct of ^{3}MBT with styrene. TD-DFT calculations provided in Figure S8 of the SI support this analysis: ^{3}[MBT-St] is computed to have an absorption maximum at 380 nm with oscillator strength f = 0.12 and features that extend to ~700 nm, whereas the triplet styrene is predicted to show an absorption band centred at 329 nm with oscillator strength f = 0.02.

3.2.2. TVAS of MBT in styrene solution. Figure 6 shows TVA spectra of 2.1 mM MBT in styrene following 330-nm excitation, together with integrated band intensities and kinetic fits. At

Please do not adjust margins

early time delays, the spectral shapes resemble those in toluene solution, except for the presence of styrene bleach bands at 1335 cm^{-1} and 1383 cm^{-1}. The two MBT bleach bands at 1318 cm^{-1} and 1414 cm^{-1} in styrene solution recover with time constants of $\tau_1 = 13.4 \pm 0.7$ ps and $\tau_2 = 659 \pm 11$ ps for the former, and $\tau_1 = 14.7 \pm 0.8$ ps and $\tau_2 = 634 \pm 13$ ps for the latter, if biexponential fittings are employed. The timescales of the faster components are similar to those observed in toluene solution and are attributed to IC from the S_1 state to the S_0 state and subsequent vibrational cooling. However, the slower recovery component is not seen in the toluene solution, and we focus on it later in this section.

The expanded view in Figure 6(c) highlights further behaviour not seen in toluene; the MBT T_1 band at 1370 cm^{-1} decays completely with a time constant of 109 ± 8 ps, which agrees with the value deduced from TEAS experiment in styrene within the 2 SD uncertainties, and with a time constant of 106 ± 9 ps for the development of the styrene bleach band at 1335 cm^{-1}. In response to the decay of the T_1 band and the growth of the styrene bleach feature, three bands at 1264, 1307 and 1395 cm^{-1} evolve. These bands are not seen in the toluene solution in Figure 4(c) or pure styrene.[2] Formation of a triplet biradical adduct by reaction of a triplet thione and an alkene has been suggested, [10, 28, 29] and the band positions are in agreement with the computed infrared frequencies for the triplet biradical addition product ^{3}[MBT-St] provided in Table 3. We could not observe the predicted band at 1253 cm^{-1} because of its small absorption intensity and spectral overlap with the MBT bleach band centred at 1249 cm^{-1}. We therefore assigned these bands to ^{3}[MBT-St] formed by the following addition reaction at the β-position of styrene:

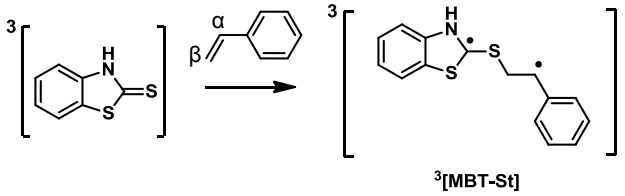

^{3}[MBT-St]

A similar addition reaction at the α-position of styrene is possible, as is an addition reaction linking the carbon atom of the thione with the α or β sites of styrene. However, we ruled out these three possibilities on the basis of the calculated fundamental infrared frequencies and the thermodynamic parameters provided in Table S3 and Figure S9 of the SI. In particular, the computed enthalpies of activation for these three reactions make them kinetically unfavourable. Further details are provided in the Supplementary Information.

One further candidate for the observed three bands in the TVA spectra is triplet styrene, formed through energy transfer from the triplet MBT. This type of triplet state energy transfer from thiones to alkenes is well-known,[47-50] but we discounted assignment to triplet styrene on the basis of experiments with the triplet sensitizer thioxanthone reported in the Supplementary Information (see Figure S10).

After reaching their maximum absorbance at ~200 ps, the ^{3}[MBT-St] bands decay gradually over our experimental time window. Fits of the integrated band intensities to eqn 2 give $\tau_3 = 1/k_3 = 138 \pm 19$ ps and $\tau_4 = 1/k_4 = 630 \pm 80$ ps for the band at 1264 cm^{-1}, $\tau_3 = 144 \pm 22$ ps and $\tau_4 = 680 \pm 100$ ps for the band at 1307 cm^{-1}, $\tau_3 = 94 \pm 19$ ps and $\tau_4 = 700 \pm 80$ ps for the band at 1395 cm^{-1}. The deduced time constants are in reasonable agreement with each other and with the time constants deduced from TEAS experiments ($\tau_3 = 105 \pm 2$ ps and $\tau_4 = 629 \pm 41$ ps). We prefer to use the time constants for the band at 1395 cm^{-1} as representative values, because the signal to noise ratio for this band is better than for the other TVAS features.

TEA spectra at late times indicate that the ^{3}[MBT-St] adduct disappears completely, but do not reveal its fate. As Figure 6 shows, we could not see any features in our chosen spectral window which grow with a time constant corresponding to the decay of ^{3}[MBT-St]. The absence of such features might be due to a low quantum yield for formation of products, or small absorption cross sections of product bands in the probe region. However, our DFT calculations suggest that one possible product, the ring-closed cyclo adduct, has bands in this region with similar infrared absorption cross sections to the ^{3}[MBT-St]. Hence we deduce that this type of product is not formed on the ns timescale, or at least is not responsible for the main losses of the ^{3}[MBT-St].

One plausible mechanism for the decay of ^{3}[MBT-St] is dissociation, resulting in ground state MBT (S_0) and the triplet excited state styrene (T_1). The MBT ground state bleaches recover on a timescale of approximately 650 ps, and this additional slow recovery of the bleach is not seen in the toluene solution. The recovery timescale is comparable to the decay of ^{3}[MBT-St], and >90% bleach recovery is observed. Moreover, the styrene bleach band at 1335 cm^{-1} illustrated in the inset to Figure 6(a) does not show any recovery, discounting the possibility for re-formation of ground state styrene. Based on these observations, and the fast IC from the S_1 state of MBT to the S_0 state characterized in Section 3.1, the kinetic model illustrated in Figure 7 is proposed for MBT ground-state recovery in styrene solution. The predicted Gibbs free energy changes provided in Figure 7 support the above discussion: the dissociation of ^{3}[MBT-St] favours MBT (S_0) + styrene (T_1), which is energetically preferred to MBT (T_1) + styrene (S_0). The mechanism of this dissociation involves a curve crossing between two triplet states, one with MBT (T_1) + St (S_0) character and the other with MBT (S_0) + St (T_1) character. Figure 8 shows calculated PECs for these two states, and the crossing which occurs at short MBT – St separations in the vicinity of the ^{3}[MBT-St] adduct. The dissociation of the ^{3}[MBT(S_0)-St(T_1)] adduct to MBT (S_0) + St (T_1) is an activated process so will be hindered by quenching of the excess internal energy of any newly formed adducts by the solvent bath. However, our calculations identify a lower energy pathway to a more loosely bound MBT (S_0) + St (T_1) complex which is also shown in Fig. 8 and could account for the observed decay of the adduct spectral features. This complex is described in further detail in the Supplementary Information, and has computed IR band frequencies that overlap the MBT (S_0) bleach features, thereby accounting for the recovery of these bleaches over timescales of several hundred ps.

 This journal is © The Royal Society of Chemistry 20xx

Please do not adjust margins

Please do not adjust margins

The integrated band intensity of the MBT bleach at 1414 cm^{-1} was modelled using the scheme in Figure 7 with fixed values of k_5 = 1/12 ps^{-1}, k_6 = 1/94 ps^{-1} and k_7 = 1/701 ps^{-1}, with all values deduced from our preceding analysis and fixed in the model, and the outcome is shown in Figure 9. The modelled data agree well with the experimental band intensity variation, which supports the proposed decay mechanism of ^{3}[MBT-St] to ground state MBT and triplet styrene as specified in eqn 2.

Conclusions

The photochemical dynamics of MBT have been investigated by a combination of transient electronic absorption spectroscopy and transient vibrational absorption spectroscopy with sub-picosecond time resolution. A formation mechanism is proposed for the first excited triplet state of MBT in methanol, toluene and styrene solutions, and in the latter case a biradical adduct is identified as an intermediate in the triplet quenching.

Photoexcitation of MBT by 330-nm ultraviolet laser light populates mainly its second singlet excited state, but ultrafast decay to the first singlet exited state occurs within our instrument response time (150 fs). The S_1 state depopulates with a time constant of 0.4 ± 0.1 ps in methanol by competing intersystem crossing to the second triplet (T_2) excited state and internal conversion to the ground state. The T_2 state relaxes to the first triplet excited state *via* internal conversion with a time constant of 6.1 ± 0.4 ps deduced by taking an average of the rise of T_1 absorption bands and the decay of T_2 state bands in TEAS measurements. Two other mechanisms might instead explain our kinetic data: (i) direct ISC from the S_1 state to vibrationally excited levels of the T_1 state (τ_1 = 0.4 ± 0.1 ps), and subsequent vibrational cooling (τ_2 = 6.1 ± 0.4 ps); and (ii) $S_2 \rightarrow S_1$ IC (τ_1 = 0.4 ± 0.1 ps) and $S_1 \rightarrow T_1$ ISC (τ_2 = 6.1 ± 0.4 ps). The first of these mechanisms could include rapid passage through the T_2 state with sub-ps internal conversion to T_1. However, the interpretation based on a gateway T_2-state pathway with ~6 ps lifetime for $T_2 \rightarrow T_1$ IC is preferred on the basis of spectroscopic evidence and plausible timescales. The quantum yields estimated from TVA spectra are 0.58 ± 0.01 for the formation of the T_1 state (*via* the T_2 state) and 0.42 ± 0.01 for the internal conversion from S_1 to high vibrational levels of the S_0 state. The T_1 state is observed both in TEAS and TVAS experiments; it has characteristic absorption bands centred at 557 nm at UV/vis region in methanol solution and at 1370 cm^{-1} in the infrared region in toluene solution. After the population of the T_1 state, the band intensity remains constant in these solutions over our experimental timescale of 1.3 ns.

In styrene solution, the T_1 band decays completely with a time constant of 105 ± 2 ps from TEAS and 109 ± 8 ps from TVAS measurements. This decay is attributed to the reaction of the MBT T_1 state with styrene, yielding the triplet biracial addition intermediate ^{3}[MBT-St] which shows absorption bands in the infrared region at 1264, 1307 and 1395 cm^{-1}. Hence, the main quenching pathway for the MBT T_1 state in styrene solution is proposed to be via an addition reaction. The ^{3}[MBT-St] bands decay with a time constant of 700 ± 80 ps. No corresponding growth of other bands is observed in the spectral window we probed, but the decay time constant matches the almost complete recovery of MBT bleach bands. Accordingly, the decay of ^{3}[MBT-St] is attributed to slow dissociation to ground state MBT and triplet state styrene via a loosely bound complex. Triplet energy transfer from the MBT T_1 state to styrene therefore takes place through the dissociation of the ^{3}[MBT-St] biradical adduct, and competing rearrangement of the biradical to a stable addition product is not seen. The combination of TEAS and TVAS with picosecond time resolution provides a comprehensive and quantitative picture of the early time processes that occur following UV excitation of MBT in the three chosen organic solvents.

Acknowledgements

We thank the European Research Council (ERC, Advanced Grant 290966 CAPRI) for financial support. We are grateful to Dr Daniel Murdock for helpful advice on the electronic structure calculations.

References

1. H. D. De Wever, K. D. De Moor and H. Verachtert, *Appl. Microbiol. Biotechnol.*, 1994, **42**, 631-635.
2. D. Koyama and A. J. Orr-Ewing, *Phys. Chem. Chem. Phys.*, 2016, **18**, 12115-12127.
3. H. C. Kolb, M. G. Finn and K. B. Sharpless, *Angew. Chem. Int. Ed.*, 2001, **40**, 2004-2021.
4. M. Serdechnova, V. L. Ivanov, M. R. M. Domingues, D. V. Evtuguin, M. G. S. Ferreira and L. M. Zheludkevich, *Phys. Chem. Chem. Phys.*, 2014, **16**, 25152-25160.
5. M. A. Malouki, C. Richard and A. Zertal, *J. Photochem. Photobiol. A: Chem.*, 2004, **167**, 121-126.
6. B. Ellis and P. J. F. Griffiths, *Spectrochimica Acta*, 1966, **22**, 2005-2032.
7. J. P. Chesick and J. Donohue, *Acta Cryst.*, 1971, **B27**, 1441-1444.
8. G. Contini, V. Carravetta, V. D. Castro, S. Stranges, R. Richter and M. Alagia, *J. Phys. Chem. A*, 2001, **105**, 7308-7314.
9. G. Contini, V. D. Castro, S. Stranges, R. Richter and M. Alagia, *J. Phys. Chem. A*, 2002, **106**, 2833-2837.
10. A. Maciejewski and R. P. Steer, *Chem. Rev.*, 1993, **93**, 67-98.
11. R. P. Steer and V. Ramamurthy, *Acc. Chem. Res.*, 1988, **21**, 380-386.
12. J. A. Mondal, H. N. Ghosh, T. Mukherjee and D. K. Palit, *J. Phys. Chem. A*, 2006, **110**, 12103-12112.
13. A. H. Maki, P. Svejda and J. R. Huber, *Chem. Phys.*, 1978, **32**, 369-380.
14. J. Kamphuis, H. J. T. Bos, R. J. Visser, B. H. Huizer and C. A. G. O. Varma, *J. Chem. Soc., Perkin Trans. 2*, 1986, 1867-1874.
15. K. Bhattacharyya, V. Ramamurthy and P. K. Das, *J. Phys. Chem.*, 1987, **91**, 5626-5631.
16. G. Cui and W. Fang, *J. Chem. Phys.*, 2013, **138**, 044315.
17. L. Martínez-Fernández, I. Corral, G. Granucci and M. Persicob, *Chem. Sci.*, 2014, **5**, 1336-1347.
18. M. Pollum and C. E. Crespo-Hernández, *J. Chem. Phys.*, 2014, **140**, 071101.

Please do not adjust margins

Please do not adjust margins

19. S. Mai, P. Marquetand and L. González, *J. Phys. Chem. A*, 2015, **119**, 9524.
20. M. Pollum, S. Jockusch and C. E. Crespo-Hernández, *Phys. Chem. Chem. Phys.*, 2015, **17**, 27851-27861.
21. S. Mai, P. Marquetand and L. González, *J. Phys. Chem. Lett.*, 2016, **7**, 1978-1983.
22. C. Reichardt, C. Guo and C. E. Crespo-Hernández, *J. Phys. Chem. B*, 2011, **115**, 3263.
23. S. Bai and M. Barbatti, *J. Phys. Chem. A*, Accepted in 2016.
24. C. Reichardt and C. E. Crespo-Hernández, *Chem. Commum.*, 2010, **46**, 5963-5965.
25. L. Martínez-Fernández, L. González and I. Corral, *Chem. Commun.*, 2012, **48**, 2134-2136.
26. M. Pollum, S. Jockusch and C. E. Crespo-Hernández, *J. Am. Chem. Soc.*, 2014, **136**, 17930-17933.
27. Y. Harada, C. Okabe, T. Kobayashi, T. Suzuki, T. Ichimura, N. Nishi and Y. Xu, *J. Phys. Chem. Lett.*, 2010, **1**, 480-484.
28. M. M. Alam, M. Fujitsuka, A. Watanabe and O. Ito, *J. Chem. Soc., Perkin Trans. 2*, 1998, 817-824.
29. M. M. Alam, M. Fujitsuka, A. Watanabe and O. Ito, *J. Phys. Chem. A*, 1998, **102**, 1338-1344.
30. A. Ohno, Y. Ohnishi, M. Fukuyama and G. Tsuchihashi, *J. Am. Chem. Soc.*, 1968, **90**, 7038-7043.
31. R. Bonneau and B. Herran, *Laser Chem.*, 1984, **4**, 151-170.
32. G. M. Roberts, H. J. B. Marroux, M. P. Grubb, M. N. R. Ashfold and A. J. Orr-Ewing, *J. Phys. Chem. A*, 2014, **118**, 11211-11225.
33. M. J. Frisch, G. W. Trucks, H. B. Schlegel, G. E. Scuseria, M. A. Robb, J. R. Cheeseman, G. Scalmani, V. Barone, B. Mennucci, et al., *Gaussian 09, Gaussian Inc., Wallingford CT*, 2009.
34. C. Lee, W. Yang and R. G. Parr, *Phys. Rev. B*, 1988, **37**, 785-789.
35. A. D. Becke, *J. Chem. Phys.*, 1993, **98**, 5648-5652.
36. T. Yanai, D. P. Tew and N. C. Handy, *Chem. Phys. Lett.*, 2004, **393**, 51-57.
37. S. Grimme, J. Antony, S. Ehrlich and H. Krieg, *J. Chem. Phys.*, 2010, **132**, 154104.
38. H.-J. Werner, P. J. Knowles, G. Knizia, F. R. Manby, M. Schütz, P. Celani, T. Korona, R. Lindh, A. Mitrushenkov, et al., *MOLPRO, version 2010.1, a package of ab initio programs. see* http://www.molpro.net.
39. T. H. J. Dunning, *J. Chem. Phys.*, 1989, **90**, 1007-1023.
40. D. E. Woon and T. H. J. Dunning, *J. Chem. Phys.*, 1993, **98**, 1358-1371.
41. M. P. Grubb, A. J. Orr-Ewing and M. N. R. Ashfold, *Rev. Sci. Instrum*, 2014, **84**, 064104.
42. M. A. El-Sayed, *J. Chem. Phys.*, 1962, **36**, 573-574.
43. H. Kuramochi, T. Kobayashi, T. Suzuki and T. Ichimura, *J. Phys. Chem. B*, 2010, **114**, 8782-8789.
44. K. Taras-Goślińska, G. Burdziński and G. Wenska, *J. Photochem. Photobiol. A: Chem.*, 2014, **275**, 89-95.
45. D. Murdock, R. A. Ingle, I. V. Sazanovich, I. P. Clark, Y. Harabuchi, T. Taketsugu, S. Maeda, A. J. Orr-Ewing and M. N. R. Ashfold, *Phys. Chem. Chem. Phys.*, 2016, **18**, 2629-2638.
46. O. Brede, F. David and S. Steenken, *J. Photochem. Photobiol. A: Chem.*, 1996, **97**, 127-131.
47. *Handbook of Photochemistry, 3rd Edn. CRC Press, Boca Raton 2006*.
48. L. J. A. Martins and T. J. Kemp, *J. Chem. Soc., Faraday Trans. 1*, 1982, **78**, 519-531.
49. C. V. Kumar, L. Qin and P. K. Das, *J. Chem. Soc., Faraday Trans. 2*, 1984, **80**, 783-793.
50. K. Bhattacharyya, P. K. Das, V. Ramamurthy and V. P. Rao, *J. Chem. Soc., Faraday Trans. 2*, 1986, **82**, 135-147.

This journal is © The Royal Society of Chemistry 20xx

Please do not adjust margins

Figure 1

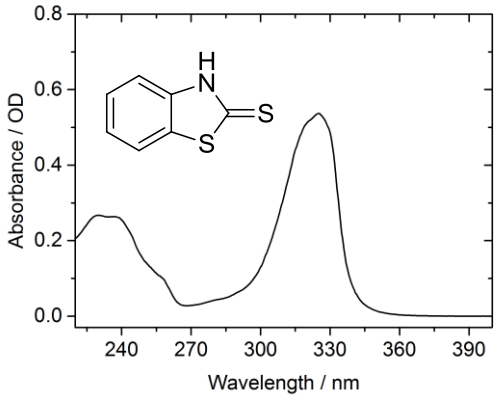

Figure 1: Steady state UV/vis absorption spectrum of 0.56 mM MBT in methanol. The spectrum was taken using a 380 µm pathlength sample.

Please do not adjust margins

Table 1: Calculated Vertical Excitation Energies and Transition Dipole Moments for MBT, Obtained at the CASPT2(8/7)/aug-cc-pVTZ and CASSCF(8/7)/aug-cc-pVTZ Levels of Theory.

Transition	Excitation energy / eV	Excitation wavelength / nm	Transition dipole moment / Debye
S_1 (nπ*)	3.24	383	0.0
S_2 (ππ*)	3.69	336	5.5
S_3 (ππ*)	3.85	322	3.7
T_1 (ππ*) [a]	2.94	422	-
T_2 (nπ*) [a]	3.14	394	-

[a] The specified orbital characters of these states are appropriate for the geometries in the vertical Franck-Condon region.

This journal is © The Royal Society of Chemistry 20xx

Please do not adjust margins

Figure 2

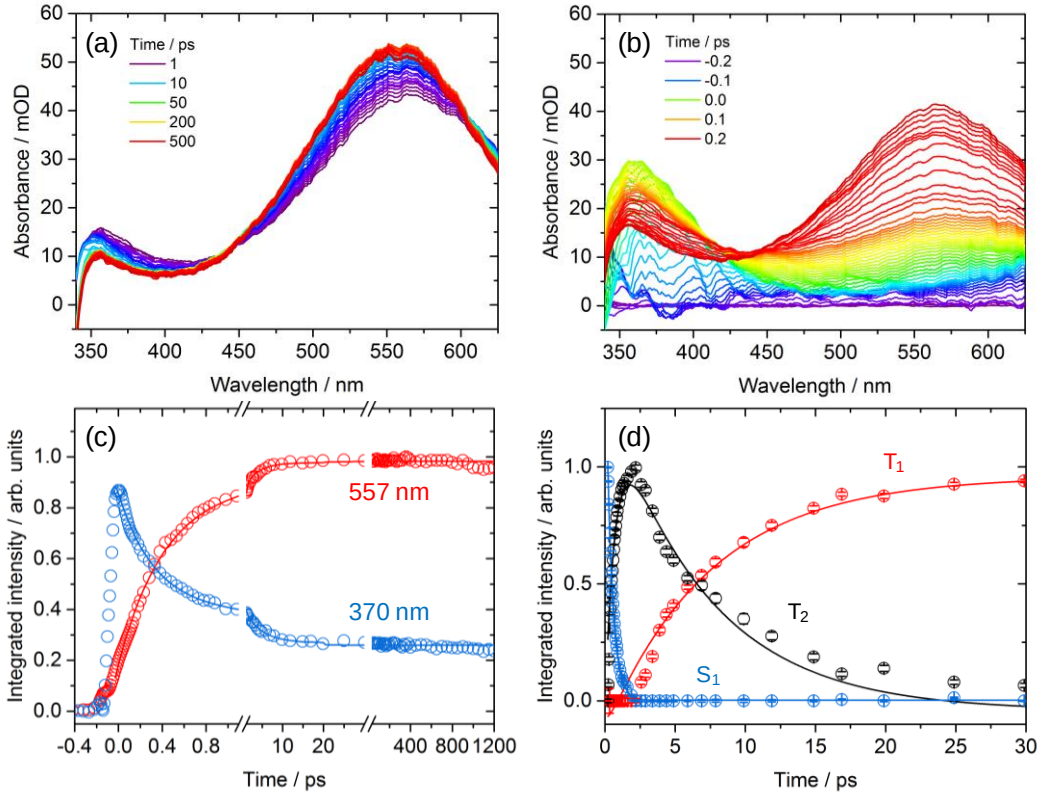

Figure 2: (a) Transient electronic absorption spectra of 0.56 mM MBT in methanol from 1 – 500 ps after 330-nm excitation. (b) TEA spectra for the first 1.0 ps. (c) Time-dependence of the bands at 557 nm (red) and 370 nm (blue). The solid lines represent exponential fittings of the band intensities. (d) Time-dependence of the S_1 (blue), T_1 (red) and T_2 state (black) absorptions obtained by spectral decomposition using the method described in the main text. The solid lines represent a global fitting of the three integrated band intensities to eqn 1.

Figure 3

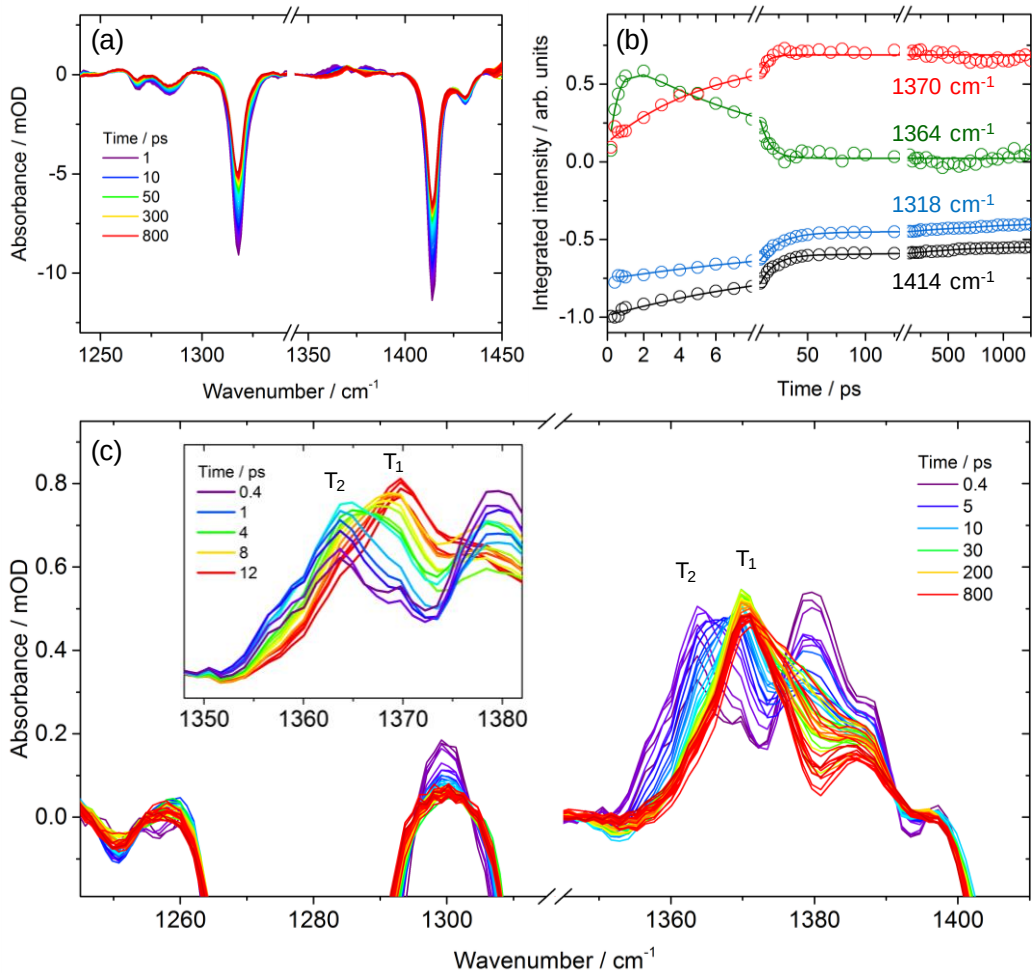

Figure 3: (a) Transient vibrational absorption spectra of 2.1 mM MBT in toluene solution following 330-nm excitation (b) Time-dependence of band intensities at 1318 (blue), 1364 (green), 1370 (red) and 1414 cm^{-1} (black). The band intensities at 1364 cm^{-1} and 1370 cm^{-1} are multiplied by a factor of 10 for clarity. The solid lines represent exponential fittings of the integrated band intensities for the bands at 1318, 1370 and 1414 cm^{-1}, and a fitting of the intensity at 1364 cm^{-1} to eqn 1. (c) Expanded view of the TVA spectra which highlights transient features assigned to the T_2 and T_1 states of MBT. The inset shows the rapid evolution of the triplet-state bands at short time delays.

This journal is © The Royal Society of Chemistry 20xx

Please do not adjust margins

Table 2: Calculated Fundamental Infrared Transition Frequencies and Intensities, and Observed Infrared Frequencies for Singlet and Triplet States of MBT.

	Calculation [a]		Experiment
	Frequency [b] / cm^{-1}	Intensity [c] / km mol^{-1}	Frequency / cm^{-1}
MBT S_0	1272	45	1283
	1316	116	1318
	1403	239	1414
	1450	52	1432
MBT T_1	1312	18	-[d]
	1372	8	1370

[a] Calculations used the Gaussian 09 package and the B3LYP functional with the 6-311++G(3df,3pd) basis set.
[b] Calculated infrared frequencies over our experimental probe region (1240 cm^{-1} - 1450 cm^{-1}). The infrared positions presented in the table are corrected by a linear function obtained by comparing the experimental and calculated frequencies of BSSB.[2]
[c] Only calculated bands with band intensities greater than 5 km mol^{-1} are shown.
[d] Not seen due to spectral overlaps with the MBT bleach band at 1314 cm^{-1} (see Figure S6 for a steady state FT-IR spectrum of MBT in styrene solution).

Please do not adjust margins

Please do not adjust margins

Figure 4

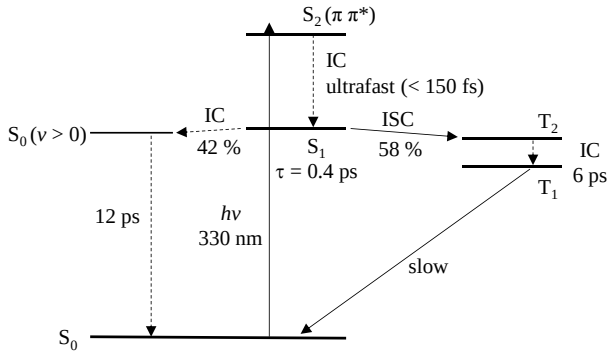

Figure 4: Proposed scheme for the formation of the MBT T_1 state and related relaxation mechanisms following UV photoexcitation. The scheme assumes that IC from the S_2 state to the S_1 state is ultrafast and is complete within our instrument response function of ~150 fs. The time constants shown in the figure are deduced by taking an average of values mentioned in the main text. The decay pathway from the T_1 state to the S_0 state is out of our probe temporal window, and is either a radiative process (phosphorescence) or a non-radiative process *via* ISC to high vibrational levels of the S_0 state.

This journal is © The Royal Society of Chemistry 20xx

Please do not adjust margins

where the decay of the T_1 state is complete. This method assumes that each spectral band shape does not change further with time.

Figure 5

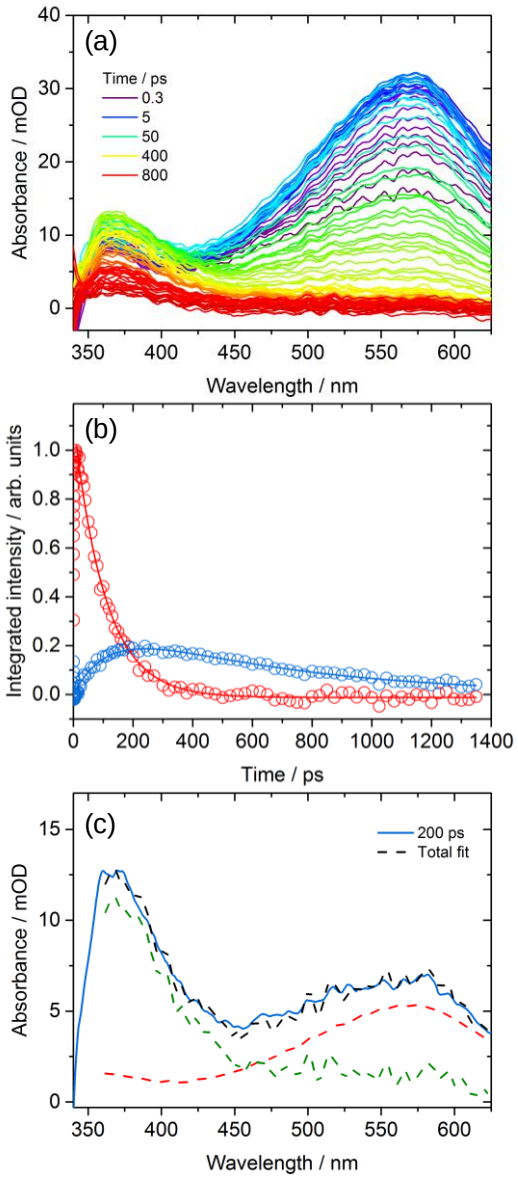

Figure 5: (a) Transient electronic absorption spectra of 0.56 mM MBT in styrene solution following 330-nm excitation. (b) Time-dependence of the T_1 state of MBT (red) and the band peaking at around 370 nm (blue). The solid lines represent exponential fitting for the T_1 state spectra (red), and fitting of integrated band intensities to a sequential kinetic model, eqn 2 (blue). The time-dependent band intensities were obtained by spectral decomposition with the KOALA program.[41] An example of this spectral decomposition is shown in (c) for a transient spectrum obtained at a time delay of 200 ps. The spectral decomposition was carried out using basis spectra corresponding to the absorption spectrum of the T_1 state of MBT at 10 ps (red dashed line), where this band reaches its maximum intensity, and the absorption spectrum at 800 ps (green dashed line),

Please do not adjust margins

Figure 6

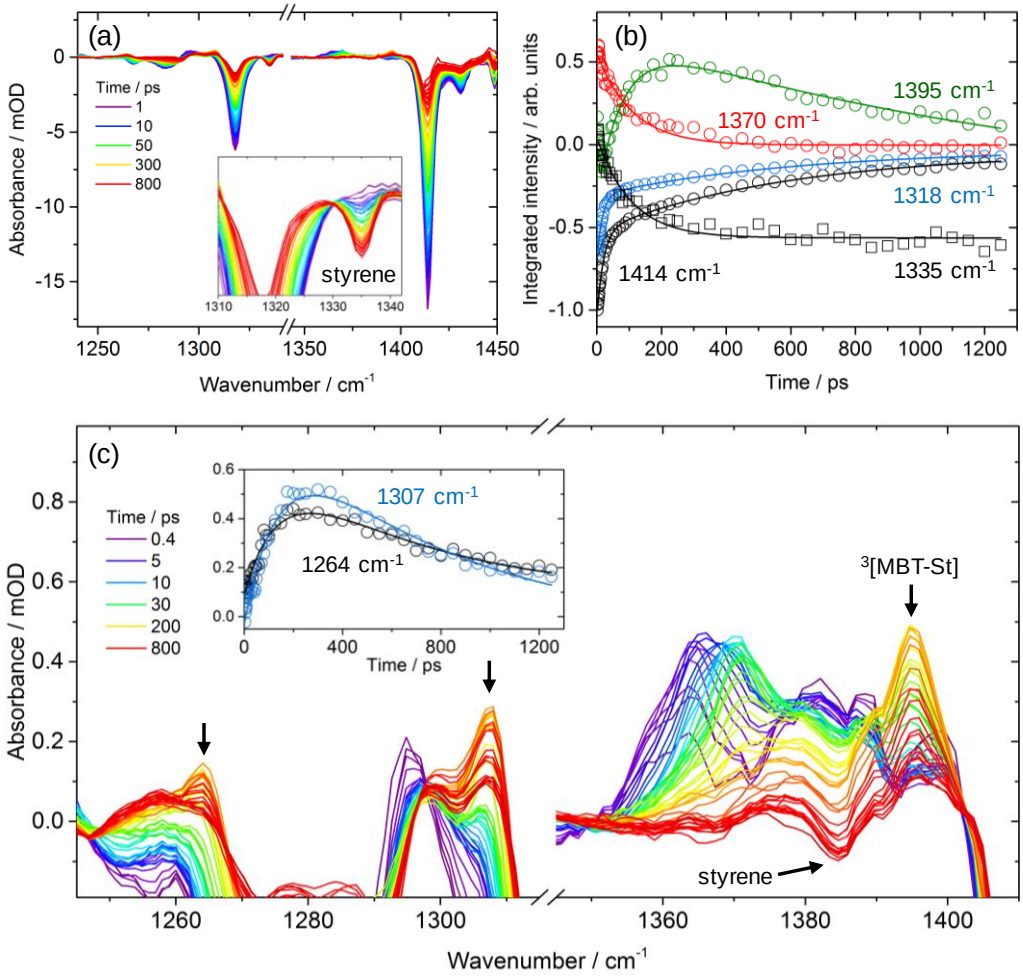

Figure 6: (a) Transient vibrational absorption spectra of 2.1 mM MBT in styrene solution following 330-nm excitation. Inset: expanded view of the spectra. (b) Time-dependence of band intensities at 1318 (blue), 1335 (black squares) 1370 (red), 1395 (green) and 1414 cm^{-1} (black circles). The band intensities at 1335, 1370 and 1395 cm^{-1} are multiplied by a factor of 10 for clarity. The solid lines represent single exponential fitting of the integrated intensity for the band at 1370 cm^{-1}, biexponential fittings for the bands at 1318 cm^{-1} and 1414 cm^{-1}, and a fit of the integrated band intensity at 1395 cm^{-1} to eqn 2. (c) Expanded view of the TVA spectra. Inset: time-dependences of the bands at 1264 cm^{-1} (black) and 1307 cm^{-1} (blue). The solid lines are fits of the intensities to eqn 2. The band intensities at 1370 cm^{-1} and 1395 cm^{-1} are multiplied by a factor of 20 for clarity.

This journal is © The Royal Society of Chemistry 20xx

Please do not adjust margins

Table 3: Calculated Fundamental Infrared Transition Frequencies and Intensities, and Observed Infrared Band Frequencies for the ^{3}[MBT-St] Adduct.

	Calculation [a]		Experiment
	Frequency / cm^{-1}	Intensity / km mol^{-1}	Frequency / cm^{-1}
^{3}[MBT-St]	1253	20	-[b]
	1262	26	1264
	1311	60	1307
	1389	60	1395
	1444	75	-[b]

[a] The calculations were performed, and the computed frequencies were corrected in the same way as described for Table 2.
[b] Not seen due to spectral overlaps with the MBT bleach band at 1249 cm^{-1} and with the styrene solvent band centred at 1450 cm^{-1} (see Figure S6 of the SI for steady state FT-IR spectra of styrene and MBT in styrene solution).

Please do not adjust margins

Figure 7

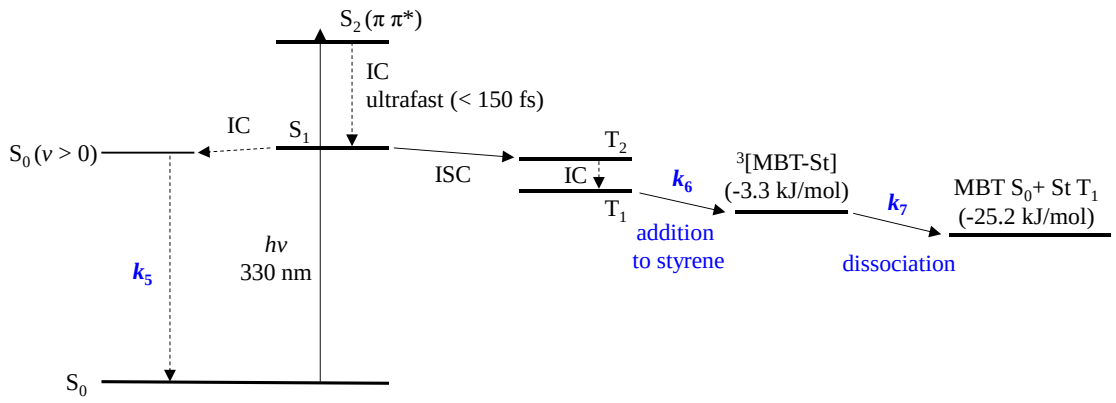

Figure 7: Proposed kinetic model for the recovery of MBT ground state. Energies in parentheses represent Gibbs free energy changes relative to the sum of the energies of the MBT (T_1) state and styrene (S_0), and were obtained by DFT calculations at the B3LYP/6-311++G(3df,3pd) level.

This journal is © The Royal Society of Chemistry 20xx

Please do not adjust margins

Figure 8

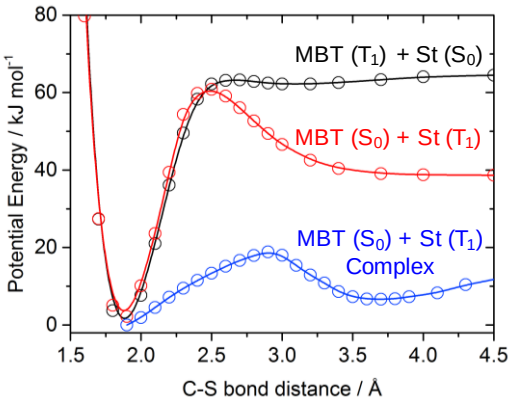

Figure 8: Potential energy curves as a function of distance from the thione sulfur atom to the carbon atom at the β position of styrene, obtained at the CAM-B3LYP-D3/6-311+G(d,p) level of theory. Black: MBT (T_1) + St (S_0) state; red: MBT (S_0) + St (T_1) state; blue: MBT (S_0) + St (T_1) complex state.

Please do not adjust margins

Figure 9

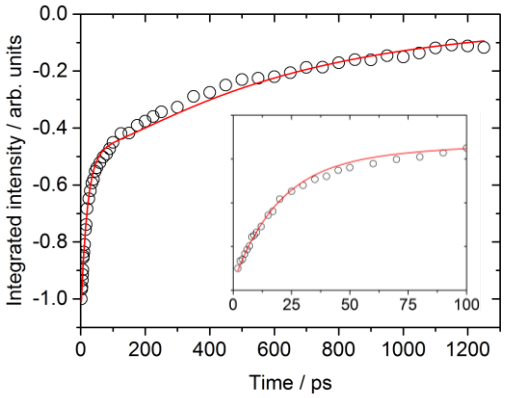

Figure 9: Time-dependence of the integrated intensity of the MBT bleach band at 1414 cm^{-1}. Open circles are experimental measurements and the solid line is a model of this band intensity described in the main text. Inset: expanded view of the first 100 ps.

This journal is © The Royal Society of Chemistry 20xx

Please do not adjust margins

Please do not adjust margins

Table of Contents Graphic

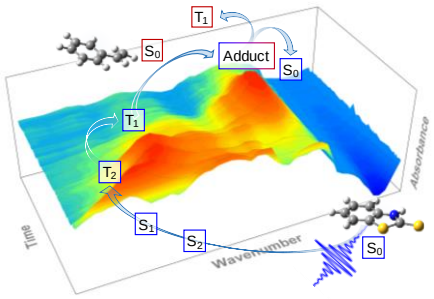

An adduct-mediated triplet energy transfer from a triplet thione to an alkene is observed with time-resolved vibrational absorption spectroscopy.

This journal is © The Royal Society of Chemistry 20xx

Please do not adjust margins